Sensors and Actuators B 233 (2016) 654–666

Contents lists available at ScienceDirect

Sensors and Actuators B: Chemical

journal homepage: www.elsevier.com/locate/snb

Mimetic biosensors composed by layer-by-layer films of phospholipid, phthalocyanine and silver nanoparticles to polyphenol detection

Priscila Alessio[a,*], Cibely S. Martin[a], Jose A. de Saja[b], Maria L. Rodriguez-Mendez[c]

[a] Faculdade de Ciências e Tecnologia, UNESP Univ. Estadual Paulista, Presidente Prudente, 19060-080, SP, Brazil
[b] Departamento de Física de la Materia Condensada, Facultad de Ciencias, Universidad de Valladolid, 47011 Valladolid, Spain
[c] Grupo UVAsens. Escuela de Ingenierías Industriales, Universidad de Valladolid, 47011 Valladolid, Spain

ARTICLE INFO

Article history:
Received 22 January 2016
Received in revised form 15 April 2016
Accepted 25 April 2016
Available online 26 April 2016

Keywords:
Mimetic biosensor
Layer-by-layer films
Phospholipid
Iron tetrasulfonated phthalocyanine
Silver nanoparticles
Polyphenol detection

ABSTRACT

Highly selective and sensitive modified electrodes have been the focus of many studies in sensing applications. Gene or enzymatic biosensors are greatly effective in this context, but they are often fragile and expensive. An alternative to these systems is the use of mimetic systems such as artificial enzyme immobilized in a matrix formed by thin films, for which the electrostatic layer-by-layer (LbL) technique has been widely applied. Here, the formation of bilayers or trilayers combining a cationic electrolyte (poly(allylamine) hydrochlorate, PAH), an anionic metallic complex (iron tetrasulfonated phthalocyanine, FeTsPc), an anionic phospholipid 1,2-dipalmitoyl-sn-3-glycero-(phosphor-rac-(1-glycerol), DPPG) and silver nanoparticles (AgNPs) arranged as (PAH/FeTsPc + DPPG)n and (PAH/FeTsPc + DPPG/AgNP)n was structurally and morphologically characterized. The electrostatic interaction of PAH, FeTsPc, and DPPG molecules were identified as the driven forces that allow the LbL film growth. The incorporation of AgNPs in the LbL films makes possible to active the surface enhanced resonant Raman scattering (SERRS) effect. The LbL films were evaluated as a sensor to catechol by cyclic voltammetry and impedance spectroscopy. The presence of AgNPs enhances the electrocatalytic activity of FeTsPc in the film to catechol oxidation. The $(PAH/FeTsPc + DPPG/AgNP)_5$ LbL film presented a linear concentration range for catechol detection from 2 up to 100 μM, with a limit of detection of 0.87 μM. The distinction of catechol concentrations as well as discrimination among catechol, gallic and vanillic acid aqueous solutions was efficiently performed by principal component analysis (PCA) from impedance spectroscopy measurements. The LbL films here evaluated showed suitable properties to be applied as mimetic biosensors. The sensor was applied to polyphenol determination in green tea samples by standard addition showing high selectivity to catechol compared with results from Folin-Ciocalteu method.

1. Introduction

Polyphenols are one of the most powerful bioactive compounds to help to prevent chronic diseases, due to their great antioxidant properties acting against cell oxidative stress [1]. Thus, the detection of phenolic compounds is of great interest not only in medical but also in environmental and food industry [2,3]. Among the available sensors to quantify polyphenols, biosensors have been pointed as the best option as selective and sensitive method [4]. However, the biosensors have some limitations, such as low enzyme stability, short lifetime, significant inhibition caused by product reactions, cost (relatively expensive), and the special care of storage. To overcome this kind of limitations, organic thin films have been applied as a functional mimetic enzyme in sensing applications [5–7]. Among the organic thin films used in sensing applications, the metallic phthalocyanines (MPc) are known as electronic mediators and due to structural similarity of these molecules with the heme prosthetic groups of enzymes make them suitable for applications in synthetic models of biosensors [8]. Besides, MPc has shown interesting electrocatalytic effects and properties as mimetic natural enzymes toward phenol detection, which make the phthalocyanines potential candidates to develop mimetic biosensors [9,10]. The layer-by-layer (LbL) technique has been widely used to assembly these mimetic biosensors forming thin films. For instance, Fernandes et al., used poly(allylamine hydrochlroride), PAH, and

* Corresponding author.
E-mail address: prialessio@gmail.com (P. Alessio).

http://dx.doi.org/10.1016/j.snb.2016.04.139
0925-4005/

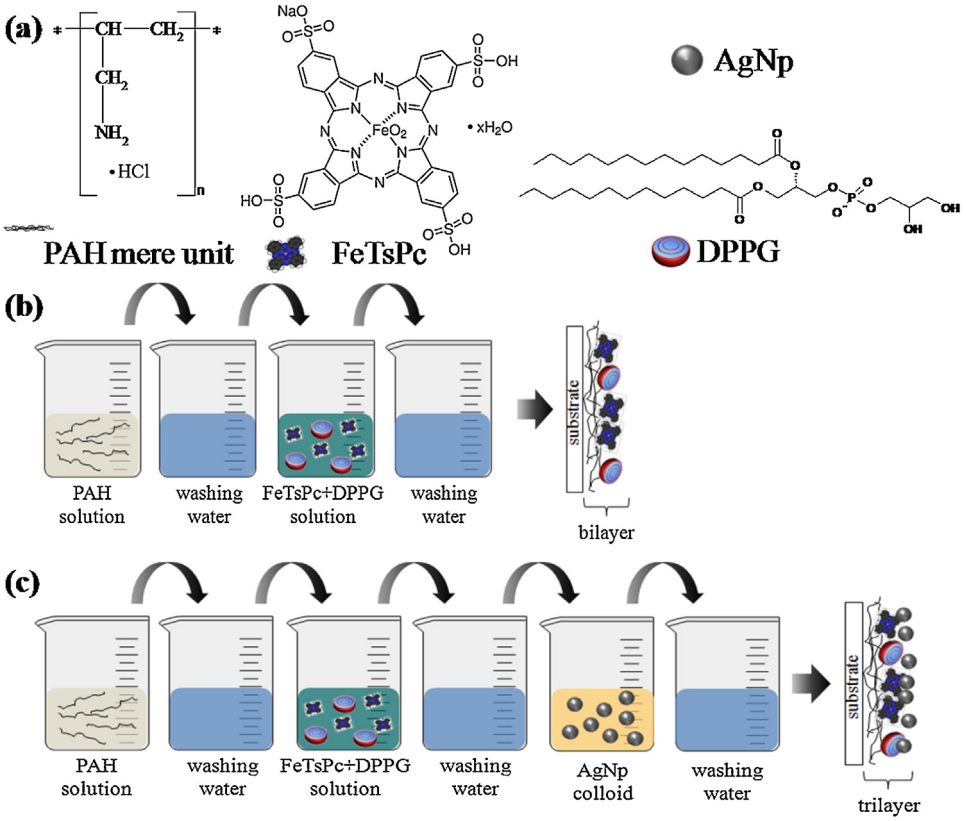

Fig. 1. schemes of the (a) molecular structures of PAH (mere), FeTsPc and DPPG. Illustration of the LbL film fabrication with (b) bilayers and (c) trilayers.

lutetium bisphthalocyanine, $LuPc_2$, LbL films as a mimetic biosensor for phenol detection [7].

Recently, AuNPs and phthalocyanines have been successfully combined to obtain electrochemical sensors with improved electrocatalytic properties [11,12]. Such sensors have been prepared by electrospinning or spin coating. A synergistic electrocatalytic effect towards hydroquinone has been observed in electrodes combining phthalocyanines and AuNPs in LB films [13]. Here, we describe the development of mimetic biosensors through LbL films based on FeTsPc mixing with DPPG and also with the incorporation of silver nanoparticles (AgNPs). This approach is chosen because the FeTsPc may act as a mimetic enzyme, the DPPG has shown good performance in sensing experiments, besides being a suitable matrix to immobilize biomolecules [14]. The incorporation of AgNPs may improve the catalytic properties of the electrochemical and electrical impedance system [15]. Moreover, AgNp can promote the surface-enhanced Raman scattering (SERS) phenomenon, which is a vibrational spectroscopic technique that provides structural information and can also be applied as sensing tool [16].

In this work, the LbL films composed by bilayers (PAH/FeTsPc + DPPG)n or trilayers (PAH/FeTsPc + DPPG/AgNp)n was evaluated as sensors to polyphenol determination. Initially, the growth, the morphology and molecular interactions for both LbL films were investigated by UV–vis absorption, Raman, FEG-SEM and FTIR spectroscopy. The performance of the LbL films in catechol (diphenol), vanillic acid (monophenol) and gallic acid (triphenol) standard solution was studied using electrochemical (cyclic voltammetry) and electrical (impedance spectroscopy) techniques. The distinction between polyphenol solutions was done through the principal component analysis (PCA) from impedance spectroscopy measurements. The electroanalytical parameters and the polyphenol quantification in green tea samples are carried out using the catechol as standard.

2. Materials and methods

2.1. Reagents

Anionic phospholipid DPPG 1,2-dipalmitoyl-sn-3-glycero-(phosphor-rac-(1-glycerol), MW = 745 g/mol, purity >99%) was purchased from Avanti Polar Lipids Inc. Iron(III) phthalocyanine 4,4′,4″,4‴ tetrasulfonic acid (FeTsPc, MW = 942.60 g/mol), Poly(allylamine hydrochloride) (PAH, MW = 56×10^3 g/mol), sodium citrate ($C_6H_5Na_3O_7$. $2H_2O$, MW = 294.1 g/mol) and silver nitrate ($AgNO_3$, MW = 169.88 g/mol) were acquired from Sigma-Aldrich Co., Ultrapure water (18.2 MΩ cm and ~pH 6.5) acquired from a Milli-Q system, model Simplicity, was used to prepare all LbL film solutions (and dispersion in case of DPPG). Fig. 1(a) shows the molecular structures of PAH (mere), FeTsPc and DPPG. Catechol, gallic acid, vanillic acid (Sigma-Aldrich Co.) were used on sensorial measurements.

2.2. Solutions and LbL film preparation

The solutions and LbL films were prepared as described in references [16,17]. In general, the solutions were prepared without any special procedure: the powder was simply added to ultrapure water and the solutions were gently stirred. In the case of FeTsPc + DPPG mixed solution, the FeTsPc powder was added to the DPPG dispersion previously prepared. The LbL films were fabricated in bilayers and trilayers, by immersions of the substrate into the distinct solutions according to the following sequence: PAH solution (cationic) for 3 min → ultrapure water gently stirred to remove excess of adsorbed PAH (1 min) → FeTsPc + DPPG (anionic) for 3 min → ultrapure water to remove excess of adsorbed material (1 min). In the case of trilayers, an additional step of immersion into AgNPs colloidal solution (3 min) and subsequent ultrapure water

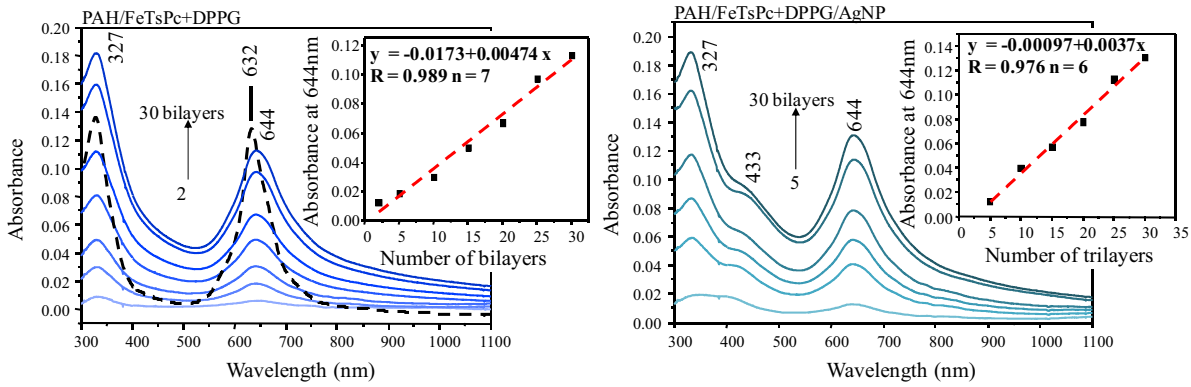

Fig. 2. UV–vis absorption spectra of (a) FeTsP + DPPG mixture in aqueous solution (dashed curve) and PAH/FeTsPc + DPPG LbL films containing different numbers of bilayers (2–30 bilayers) onto a quartz substrate. (b) UV–vis absorption spectra for PAH/FeTsPc + DPPG/AgNP LbL film containing different numbers of trilayers (5–30) onto a quartz substrate. *Insets*: increase of UV–vis absorption at 644 nm as a function of the number of (a') PAH/FeTsPc + DPPG bilayers or (b') PAH/FeTsPc + DPPG/AgNP trilayers deposited.

rinse was carried out. After that, the first bilayer or trilayer is formed and the multilayered LbL films were grown by repetition of the sequence until reaching. Fig. 1(b) illustrates the LbL film fabrication.

The AgNp colloidal solution was obtained following the synthesis methods proposed by Lee and Meisel [18], which experimental procedures are described in detail in [19]. Here, the size of AgNPs in the films was estimated between 30 and 70 nm using the software Gwyddion. However, in solution with a concentration of 1 mmol/L Ag colloid, the AgNPs present preferentially spherical shape with a size distribution in diameter ranging from 25 to 130 nm with a maximum distribution between 30 and 40 nm [20–22]. The colloidal AgNPss are negatively charged with a zeta potential of ca. −45 mV [23].

2.3. Film characterization

The growth of LbL films (from 2 up to 30 bilayers) was monitored by UV–vis absorption. The spectra between 190 and 1100 nm were collected using a Varian spectrophotometer model Cary 50. The LbL films were also characterized by FTIR and micro-Raman spectroscopy. FTIR spectra were obtained in transmission mode using a Bruker spectrometer model Vector 22, with a spectral resolution of 4 cm^{-1} and 128 scans.

Raman analysis and optical microscopy were obtained using a micro-Raman Renishaw spectrograph model in-Via equipped with a Leica microscope and CCD detector. The coupling micro-Raman (optical microscopy and Raman scattering) allows obtaining information for both morphology and chemical mapping, where the Raman spectra are obtained with a spatial resolution of approximately 1 μm (50× objective lens). The Raman mapping in two dimensions (line observed on the optical image) can be obtained by collecting spectra along a predefined line. In this case, spectra were collected along a line of 100 μm with a step of 1 μm resulting in 101 spectra. After collecting the spectra, the intensity of a particular band (1530 cm^{-1} in this work) can be plotted along the region where Raman spectra were obtained. The most intense bands are identified by clear points and less intense by darker spots on the line mapped. The Raman mapping was obtained through a computer-controlled three-axis-encoded (XYZ) motorized stage to take Raman images with a minimum step of 0.1 μm. The Raman spectra were collected using a laser line at 633 nm and 1800 grooves/mm grating with additional edge filter leading to a spectral resolution of ca. 4 cm^{-1}.

2.4. Sensing applications

Cyclic voltammetry was carried out using a μAUTOLAB potentiostat/galvanostat (GPES 4.9 Software) with a conventional three-electrode cell. The saturated Ag|AgCl/KCl electrode as reference electrode, a platinum plate as counter electrode and ITO electrodes (10 mm × 10 mm) modified with the LbL films as working electrode. The cyclic voltammograms were recorded at potential range from −1.0 to +1.0 V and scan rate of 50 mV/s with 0.1 M KCl aqueous solution as supporting electrolyte. The ITO electrodes modified with 5 bi- or tri-layers of distinct LbL films: $(PAH/DPPG)_5$, $(PAH/FeTsPc + DPPG)_5$ and $(PAH/FeTsPc + DPPG/AgNP)_5$ were also immersed into catechol, gallic acid, vanillic acid standard solution with concentration of 100 μM for evaluation of electrochemical catalytic effect in polyphenol solutions. The analytical curve and determination of polyphenol concentration in green tea sample ware carried out through ITO electrode modified with $(PAH/FeTsPc + DPPG/AgNP)_5$ LbL films using catechol as standard.

An electronic tongue consisting of three sensing units was applied to detect catechol (10^{-11}, 10^{-10}, 10^{-9} and 10^{-8} M), gallic acid (10^{-8} M) and vanillic acid (10^{-8} M) in aqueous solution (ultrapure water) via impedance spectroscopy. The impedance measurements were performed using a Solartron analyzer model 1260, at ca. 23 °C, between 1 and 10^6 Hz with input signal of 50 mV. The sensing units were prepared by coating Pt interdigitated electrodes with 5 bi or tri-layers of distinct LbL films: $(PAH/DPPG)_5$, $(PAH/FeTsPc + DPPG)_5$ and $(PAH/FeTsPc + DPPG/AgNP)_5$. The Pt interdigitated electrodes are formed by 50 pairs of digits, with dimensions of 0.5 mm length, 10 μm width, and 100 nm height, being 10 μm apart each other. The impedance data were statistically analyzed via principal component analysis (PCA).

The number of bilayers affected the electrochemical processes in LbL films containing metallophtahlocyanine derivates (MTsPc, M = Fe, Ni or Co), especially for LbL films formed with more than 5 bilayers [24,25]. However, for the LbL films studied here, containing 5 and 10 bi- or trilayers, no significant changes on electrochemical oxidation of polyphenol were observed. Thus, the sensing evaluation and application were realized using the LbL films containing 5 bi- or trilayers.

2.5. Principal component analysis (PCA)

Principal Component Analysis (PCA) is a statistical technique, non-supervised multivariate method, for the reduction of input data dimension and is largely used for exploratory data analysis. It summarizes the relevant features in a set of input data providing a lower dimension, but without loss of information of the original data. For that, it sequentially creates a set of principal components from the original data. The first principal component (PC1) provides most of the information to discriminate the input data and presents the highest variance. In the results presented here, using

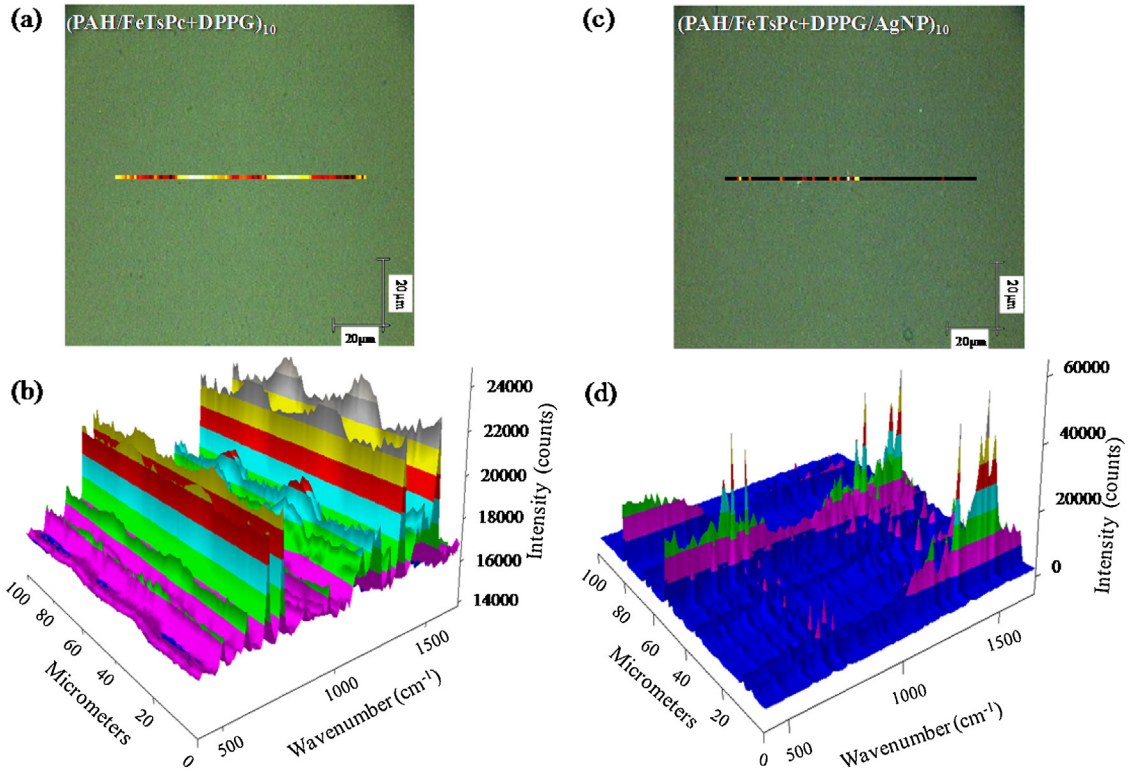

Fig. 3. optical microscopy images (500× magnification), 2D line mapping and 3D Raman line mappings for LbL films containing (a) 10 bilayers of PAH/FeTsPc + DPPG and (b) 10 trilayers of PAH/FeTsPc + DPPG/AgNP.

the first and second principal components more than 90% of the relevant information is covered in all cases. PCA was used to analyze the impedance curves and to evaluate the discrimination capability of the nanostructured sensors. The impedance curves used as data source for statistical analysis were not pre-processed, and all points measured were included in the data. In the original dataset matrixes, each line corresponds to a sensing unit (4 sensing units in triplicates = 12 lines) and each array of column correspond to one variable (5 different concentrations or 3 different polyphenols). So, as all curve points were used, each 62 column correspond to the response of each variable, being the final matrixes 12×310 and 12×248. The analyzes were carried out using the software *The Unscrambler* v 9.1 (CAMO ASA, Trondheim, Norway).

2.6. Determination of polyphenol concentration in green tea sample

Sample of green tea was obtained from local commercial brand. Amount of 1.5 g sample of green tea was added in 100 mL of hot ultrapure water (90 °C). The green tea sample solution was kept on heating for 15 min. The solution was then filtered and the volume adjusted to 100 mL. For the electrochemical experiments, 100 μL of green tea sample was added to the electrochemical cell of 25 mL, and standard addition from 0.2 up to 120 μM catechol was added in the electrochemical cell. Determination of total polyphenols content was also performed using Folin-Ciocalteu method. The Folin-Ciocalteu method was carried out similar as described by Gamella et al. [26]. Briefly, an aliquot of 10 μL of the tea sample was mixed with 250 μL of commercial Folin-Ciocalteau reagent and 1 mL of 20 wt.% sodium carbonate aqueous solution, the final volume was adjusted to 10 mL with ultrapure water. The absorbance of the color solution generated was read after about 30 min at 735 nm in 1 cm quartz cuvette. A calibration plot of absorbance in function of polyphenol concentration was performed using catechol as standard (0.05 up to 50 mg/L).

3. Results and discussion

3.1. LbL film growth monitoring

The film growth is an important parameter to be monitored since it is related to the reproducibility in the production of such films. The growth of LbL films containing FeTsPc, DPPG, and AgNPs, was monitored by UV–vis absorption measurements. Fig. 2 shows the UV–vis absorption spectra for PAH/FeTsPc + DPPG LbL film with different numbers of bilayers and for PAH/FeTsPc + DPPG/AgNP LbL film with different numbers of trilayers.

The LbL films growth show a linear relationship between the number of bilayers (PAH/FeTsPc + DPPG) or trilayers (PAH/FeTsPc + DPPG/AgNP) and the maximum absorption at 644 nm. This linear dependence shows that the same amount of material is adsorbed onto the substrate for each bi- or trilayer deposited, which is characteristic of a controlled growth of the LbL films. We can also observe that the amount of material in each layer adsorbed for both films is similar. This behavior reveals that the AgNPs do not affect the amount of FeTsPc molecules adsorbed at each layer. Growth analysis of LbL films of PAH/FeTsPc, PAH/AgNPs, and PAH/DPPG were published by our group in [16,17,27]. The growth of these films is governed by electrostatic interactions between the cationic (PAH) and anionic (FeTsPc, AgNPs or DPPG) materials. Thus, we suggest that these individual interactions govern the formation of the films studied in this work.

Fig. 2(a) also shows the UV–vis spectrum of the FeTsPc + DPPG solution (dashed line). This spectrum is assigned only to electronic transitions of FeTsPc since DPPG presents no absorption in the wavelength range studied. The absence of changes in the spectrum of FeTsPc (results not shown) reveals that there is no strong

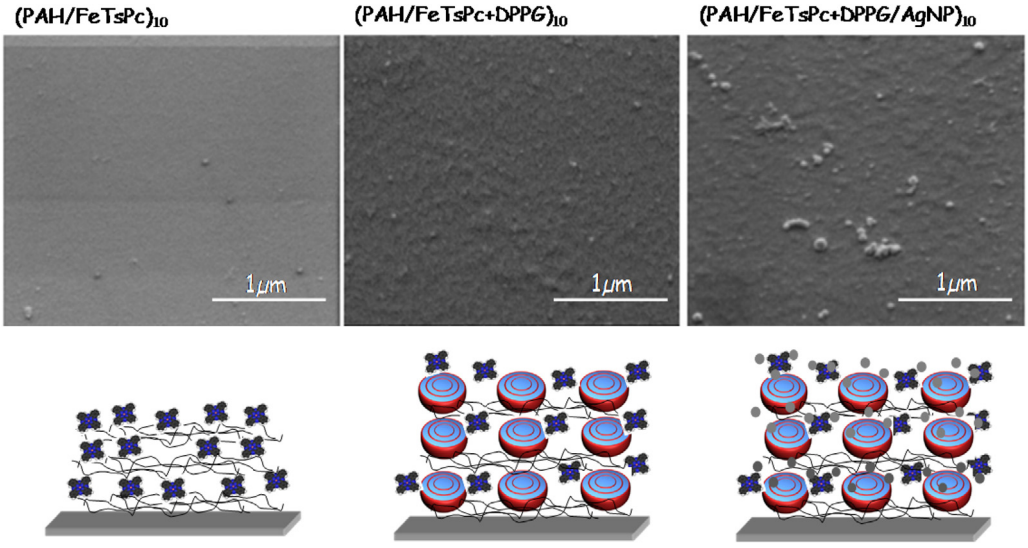

Fig. 4. FEG-SEM images for LbL films containing (a) 10 bilayers of PAH/FeTsPc (b) 10 bilayers of PAH/FeTsPc + DPPG and (c) 10 trilayers of PAH/FeTsPc + DPPG/AgNP.

chemical interaction between DPPG and FeTsPc in solution. The characteristic bands of FeTsPc are assigned to π-π* HOMO-LUMO electronic transitions, known as B-band at lower wavelengths and Q-band at higher wavelengths. In the solution, Q-band maximum absorption appears at 632 nm, which shows that the FeTsPc is preferably structured in dimeric or aggregated form since the monomeric form is expected to present maximum absorption at 670 nm (higher wavelength) [28]. Another possibility of attribution to band at 632 nm could be the μ-oxo complex formation, a dimeric form of the phthalocyanine characterized by the presence of oxygen molecules coordinated between two FeTsPc (Fe-O-Fe). However, these species are most common in alkaline solutions (pH 7–10) [29,30].

The aggregation in the LbL films are explained since the phthalocyanine macrocycle is hydrophobic and can form aggregates through π-π interactions. Briefly, the interactions governing the adsorption processes of the electrolytes in the film growth take place between the PAH positive groups and FeTsPc sulfonic negative groups. Thus, the rings, with hydrophobic characteristic, does not participate in this process and are available to interact each other by π-π stacking, favoring the formation of dimeric species and consequently aggregation in the film. A similar behavior in terms of aggregation was observed by Barbosa et al. [31] in studies on the adsorption of FeTsPc on the surface of Mg-Al hydrotalcite-like compounds in solution.

The spectra for LbL films with and without AgNPs (Fig. 2(a) and (b)) are similar, but in the case of PAH/FeTsPc + DPPG/AgNP film a band with a maximum at 443 nm related to the surface plasmon of the AgNPs [18] was observed. The similarity reveals that the addition of AgNPs in the LbL film forming a trilayer architecture (PAH/FeTsPc + DPPG/AgNP) does not change the aggregation behavior observed for the PAH/FeTsPc + DPPG films discussed above. The latter could be expected because the Ag colloid is diluted and, consequently, the AgNPs are present only in some spots on top of FeTsPc + DPPG layers, as desired and discussed in the next section through microscopy.

3.2. LbL film morphology

The morphology study of the films is important to analyze the surface coating and the aggregation, factors that influence the device performance. The morphology of the films was studied by micro-Raman measurements and scanning electron microscopy with field emission gun (FEG-SEM). Fig. 3 shows the two-dimensional mappings coupled to the optical microscopy and the three-dimensional mappings (3D) obtained for $(PAH/FeTsPc + DPPG)_{10}$ and $(PAH/FeTsPc + DPPG/AgNP)_{10}$ LbL films. The spectra collected along the line mapped are arranged side by side resulting in a 3D image. The Raman spectra are referring to the signal of FeTsPc since both DPPG and PAH show no Raman signal in films with nanometric thickness [16].

Optical microscopy (Fig. 3(a) and (b)) reveals that both LbL films present homogeneous morphology at the micrometer scale. In the Raman mapping performed for $(PAH/FeTsPc + DPPG)_{10}$ LbL films, it can be observed differences in signal intensity (about 7%) in some regions on the surface, which is related to slight differences in the concentration of material. Such differences suggest the presence of small aggregates that cannot be observed in the optical image. However, in the 3D mapping, it can be observed that all surface films present the Raman spectra with the same profile, which indicates that the surface is completely covered by the film, even in the dark spots on the 2D line. The reproducibility of Raman signal profile along the mapped line shows the chemical uniformity of the film.

In Raman mapping for the $(PAH/FeTsPc + DPPG/AgNP)_{10}$ LbL film some points have higher signal intensity. This is due to the presence of AgNPs in some points of the film, which gives rise to the phenomenon of surface-enhanced Raman scattering, or in this case surface-enhanced resonant Raman scattering (SERRS). This phenomenon can enhance the Raman signal up to 10^{10} times in specific cases and commonly amplifications of 10^3 can be easily found [32]. RRS spectrum of FeTsPc can be observed over the course of the entire mapped area (Fig. 3(d)), which indicates a good surface coverage. However, due to the large amplification in some places (AgNP aggregates) the Raman signal intensity strongly varies (Fig. 3(c)).

A detailed analysis of the film morphology for a different and more depth scale was performed. These analyzes were possible using images obtained by FEG-SEM measurements, which are shown in Fig. 4 for $(PAH/FeTsPc)_{10}$, $(PAH/FeTsPc + DPPG)_{10}$, and $(PAH/FeTsPc + DPPG/AgNP)_{10}$ LbL films. The films showed homogeneous surface, being rougher for films containing DPPG. Nevertheless, a vesicular shape expected for DPPG [17] was not observed, indicating that the vesicles were not kept in mixed solutions and/or in the $(PAH/FeTsPc + DPPG)_{10}$ LbL films. A similar result was observed by Furini et al. [33] in LbL films containing dioctadecyldimethylammonium bromide (DODAB) and nickel tetrasulfonated phthalocyanine (NiTsPc). In Furini et al. it was

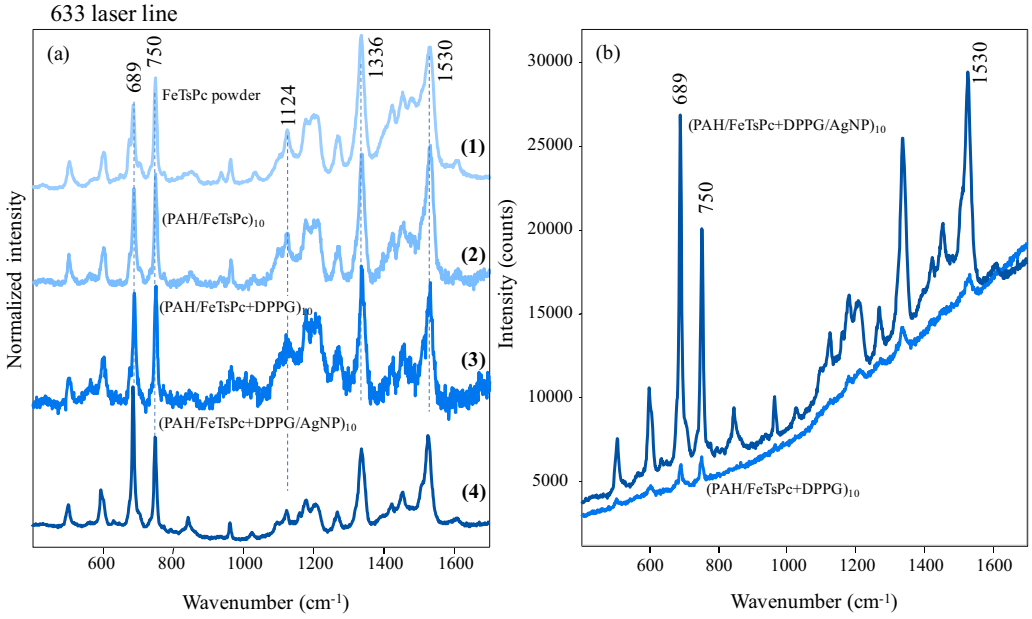

Fig. 5. (a) normalized RRS and SERRS spectra depicted from the mappings shown in Fig. 3 for the LbL films containing 10 bilayers of PAH/FeTsPc + DPPG (1); 10 trilayers of PAH/FeTsPc + DPPG/AgNP (2); and the spectra for 10 bilayers of PAH/FeTsPc (3) and FeTsPc powder (4). (b) RRS and SERRS spectra in scale for (1) and (2) in (a). 633 nm Laser Line.

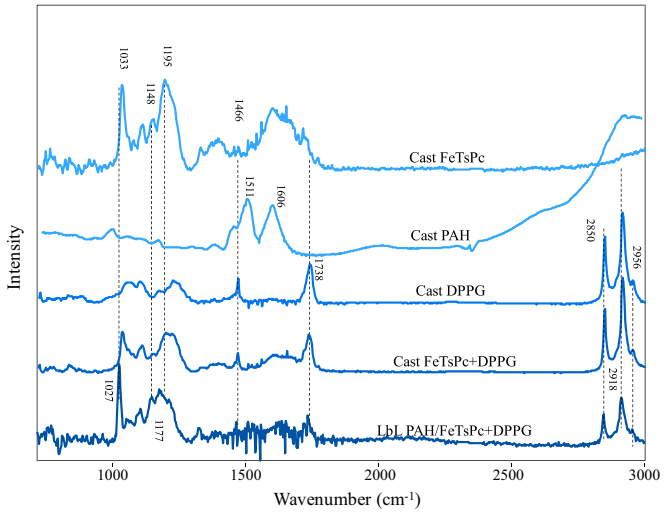

Fig. 6. FTIR spectra for FeTsPc, PAH, DPPG and (DPPG + FeTsPc) cast films and for the LbL film containing 12 bilayers of PAH/FeTsPc + DPPG. The cast and LbL films were fabricated onto the SeZn substrate surface.

observed that the lipid vesicular shape is kept in solution and in LbL film only for low phthalocyanine concentrations (below 0.05 mM) [33]. Fig. 4(c) shows that the AgNPs are present in the LbL film in both aggregates and isolated form with predominant spherical shape and are randomly distributed in the film. This result is in agreement with those observed in the Raman mapping (Fig. 3(d)) since the distribution of the AgNPs and consequently the SERS signal are spatially consistent. In the FEG-SEM images, one can observe that the whole substrate surface is covered by the film, which corroborates the Raman mapping results.

3.3. Molecular interactions

In order to study the possible molecular interactions between FeTsPc and DPPG, analysis of SERRS and RRS spectra obtained for the different films was performed. Fig. 5 shows the comparison of the Raman spectra obtained to $(PAH/FeTsPc)_{10}$, $(PAH/FeTsPc + DPPG)_{10}$, $(PAH/FeTsPc + DPPG/AgNP)_{10}$ films and for FeTsPc powder at 633 nm laser line. The assignments of the main bands of FeTsPc observed to power and LbL films are given in Table 1 [19,34,35]. It can be seen in Fig. 5(a) that the RRS and SERRS spectra obtained for all the LbL films and the powder have the same profile without significant changes considering new bands, band suppression or differences in the relative intensities of the bands. The dotted lines also show that no significant displacements of the bands are observed. The main factor that contributes to this behavior is that the 633 nm is absorbed by the FeTsPc (as seen in UV–vis – Fig. 2), which allows recording of the resonance Raman scattering (RRS) spectra, which cross section can be improved up to 10^6 in relation to conventional Raman scattering [36]. RRS spectrum for FeTsPc at 633 nm laser line is very intense and dominated by the totally symmetric modes associated with the conjugated system [37]. The similarity between the Raman spectra for all LbL films is an indication that the adsorption of the FeTsPc on the different LbL films, including with AgNPs, does not disturb significantly the electronic structure of the Pc macrocycle. This is an expected behavior since the 18 π electron system formed by the phthalocyanine is a very well delocalized system [37].

Fig. 5(b) shows the spectra for $(PAH/FeTsPc + DPPG)_{10}$ and $(PAH/FeTsPc + DPPG/AgNP)_{10}$ (spectra (1) and (2) from Fig. 5(a)) in scale to visualize the SERRS enhancement. An enhancement (30 times) was estimated using the intensities of the band at 687 cm^{-1} and considering that the power used to obtain the SERRS spectra was 50% of that used to obtain the RRS spectra. For instance, it was found enhancement factors around 50 for SERRS recorded for RhPc LB films [38].

The analysis of the electrostatic interactions between FeTsPc, DPPG, and PAH responsible for the LbL film growth is not clear using Raman spectroscopy. Based on this purpose, the FTIR measurements were also performed. Fig. 6 shows the spectra of PAH, FeTsPc, DPPG and mixing FeTsPc + DPPG cast film, as well as the spectra of LbL film containing 12 bilayers of PAH/FeTsPc + DPPG. The assignments of the bands marked with dashed lines are summarized in Table 2. Comparing the spectra, we can conclude that both materials FeTsPc and DPPG are present in the LbL film. Some DPPG

Table 1
Raman band center (cm^{-1}) and assignments for FeTsPc powder and LbL films. Raman scattering obtained using the 633 nm laser line.

FeTsPc Powder	LbL PAH/FeTsPc	LbL PAH/FeTsPc + DPPG	LbL PAH/FeTsPc + DPPG/AgNP	Assignments
1530	1531	1531 (1510s)	1529	C=C, C=N pyrrole stretching
1453	1453	1453	1455	C—N, isoindole ring stretching
1423	1422			Isoindole ring stretching
			1340 (s)	C—N breathing
1335	1335 (1338s)	1338	1338	C—N breathing, Pyrrole stretching
1269	1270	1270	1270	C—H bending
1200	1212		1208	SO_3 stretching
1178	1182		1180	C—H bending
			1162	C—H bending
1125	1125		1125	C—H bending
1033	1028		1027	Macrocycle deformation and C—H bending
963	964		964	Benzene breathing
749	750	750	751	Macrocycle deformation
686	688	689	688	Macrocycle deformation
675	676	676		Macrocycle deformation
602	602	603	602(s)	Macrocycle vibration
598(s)	599	598	597	Macrocycle vibration
504	504	504	504	Isoindole deformation

Table 2
Assignments of FTIR bands (cm^{-1}) from spectra of PAH, DPPG, FeTsPc, mixing FeTsPc + DPPG cast films and $(PAH/FeTsPc + DPPG)_{12}$ LbL film [39,59–61].

Cast PAH	*Cast* DPPG	*Cast* FeTsPc	*Cast* FeTsPc + DPPG	LbL (12 bilayers) PAH/FeTsPc + DPPG	Assignments
	2955		2956	2959	CH_3 antisymmetric stretching
	2917		2918	2918	CH_2 antisymmetric stretching
	2850		2850	2850	CH_2 symmetric stretchings
	1738		1738	1740	Carbonyl stretching
1606					NH_3^+ antisymmetric bending
1511					NH_3^+ symmetric bending
	1466				CH_2 in-plane angular deformation
	1221				P=O antisymmetric stretching
	1095				P=O symmetric stretching
		1195	1195	1177	SO_3 stretching
	1148		1148	1148	C—H bending
		1033	1033	1025	SO_3 stretching

characteristic bands can be seen at 2918 and 2850 cm^{-1} assigned to the antisymmetric and symmetric stretching of the CH_2, respectively. A weak band at 2956 cm^{-1} attributed to the antisymmetric CH_3 stretching was also observed [39]. The DPPG bands at 1221 and 1095 cm^{-1} can also be seen in the cast film spectra and are attributed to P=O (PO_4^{2-} group) antisymmetric and symmetric stretching, respectively [39]. Because these bands are overlapping with some FeTsPc bands the analysis of the interactions between DPPG and PAH through PO_4^{2-} and NH_3^+ groups are obstructed. However, Aoki et al. [17] have discussed these interactions for the PAH/DPPG LbL film growth.

The relative intensity of the band at 1195 cm^{-1} assigned to the SO_3^- stretching of FeTsPc substituent decreases in the PAH/FeTsPc + DPPG LbL film spectrum in relation to FeTsPc and FeTsPc + DPPG cast film spectra. The intensity decrease of this band confirms that the LbL film growth is governed by the electrostatic interactions between NH_3^+ groups of PAH and SO_3^- groups of FeTsPc. Another change in the spectra related to the interaction between PAH and FeTsPc through SO_3^- and NH_3^+ groups is the shift of the band at 1033 cm^{-1} in the cast film to 1027 cm^{-1} (SO_3^- stretching) in the LbL film. This electrostatic interaction was also observed in the growth of LbL films of PAH/FeTsPc [35].

3.4. Electrochemical and electrocatalytic properties in catechol, gallic acid, and vanillic acid standard solution

Fig. 7(a) shows the voltammograms in supporting electrolyte (0.1 M KCl) for LbL films of $(PAH/DPPG)_5$, $(PAH/FeTsPc + DPPG)_5$ and $(PAH/FeTsPc + DPPG/AgNP)_5$ deposited onto ITO electrodes. A redox process at ~−0.7 V *vs.* Ag/AgCl was observed to $(PAH/FeTsPc + DPPG)_5$ and $(PAH/FeTsPc + DPPG/AgNP)_5$ modified ITO electrodes. The redox process observed can be attributed to the FeTsPc macrocycle reduction and its potential is dependent on the pH solution [40–42]. It can be seen in Fig. 7(a) that the presence of DPPG or AgNP does not affect significantly the FeTsPc macrocycle reduction. The AgNP oxidation peak is observed at 0.19 V *vs.* Ag/AgCl [43].

The electrochemical catalytic effect of the LbL films was tested towards catechol, gallic acid, and vanillic acid standard solution. Fig. 7(b)–(d) shows the cyclic voltammograms of LbL films immersed in 100 μM catechol, gallic acid, and vanillic acid standard solution. The voltammograms in the presence of catechol solution show an anodic and cathodic peak associated catechol/*ortho*-benzoquinone redox couple [44,45]. The oxidation peak of catechol showed at ca. 0.28 V for $(PAH/DPPG)_5$, 0.20 V for $(PAH/FeTsPc + DPPG)_5$ and 0.16 V for $(PAH/FeTsPc + DPPG/AgNP)_5$ LbL films, respectively. The shift of the catechol redox process to minor overpotential shows that enhancement of the electrocatalytic activity of FeTsPc is improved by the AgNP, demonstrating thus the existence of synergy. The AgNP accelerate the direct electron transfer between the FeTsPc and the ITO electrode surface [46,47]. Thus, the presence of FeTsPc is responsible for catechol oxidation and the AgNP are in electron charge transfer resulting from catechol oxidation.

The voltammetric curves in the presence of gallic acid showed a large anodic peak (Fig. 7(c)) between 0.02 and 0.80 V. This redox process can be ascribed to the overlap of two redox process: (i) oxidation of galloyl group and (ii) oxidation of the third OH group [48]. The different steps for the gallic acid oxidation occur due to irreversible electron transfer process or an electron transfer process coupled with chemical reaction [49]. The films immersed in the vanillic acid solution (Fig. 7(d)), shows only one

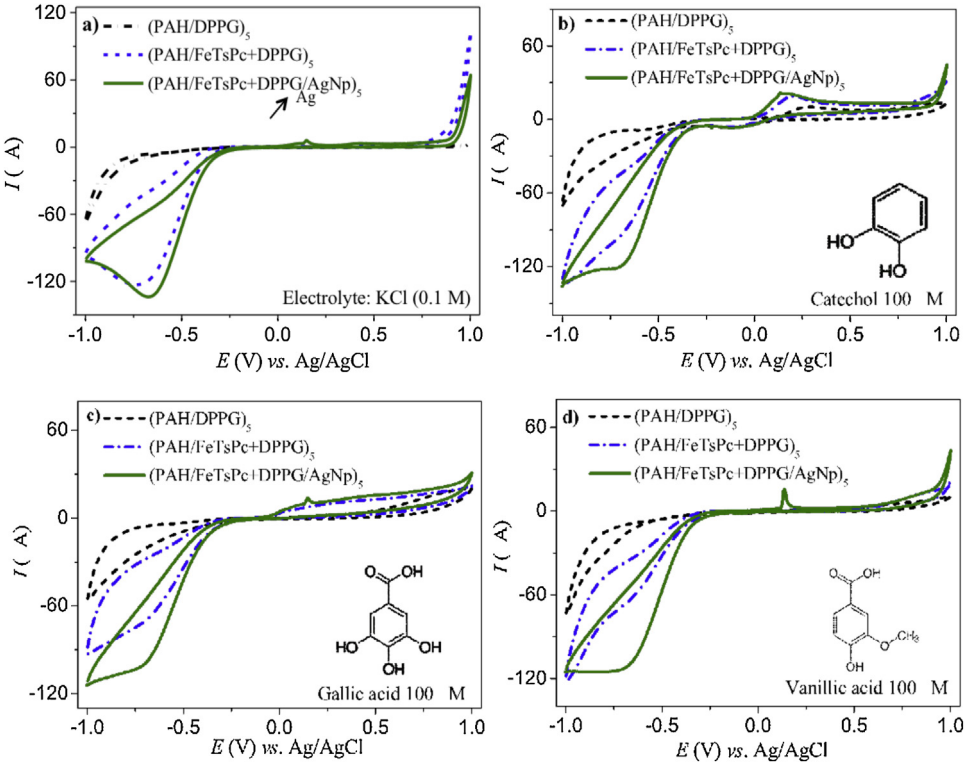

Fig. 7. cyclic voltammograms recorded to ITO electrodes modified with LbL films of $(PAH/FeTsPc)_{10}$, $(PAH/FeTsPc + DPPG)_{10}$ and $(PAH/FeTsPc + DPPG/AgNP)_{10}$ in (a) 0.1 M of KCl solution (supporting electrolyte) and in 100 μM of (b) catechol, (c) gallic acid, (d) vanillic acid standard solution containing 0.1 M KCl as supporting electrolyte. $\nu = 50$ mV/s.

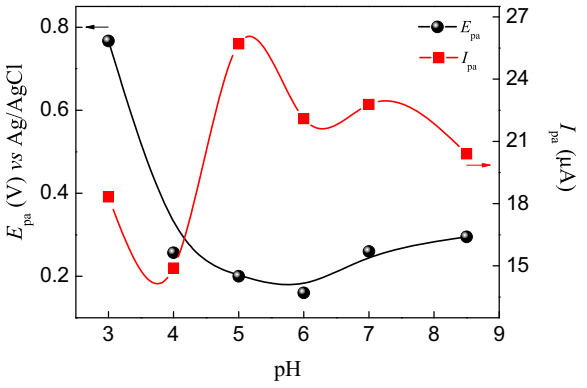

Fig. 8. effect of pH on the oxidation peak current and oxidation peak potential of catechol.

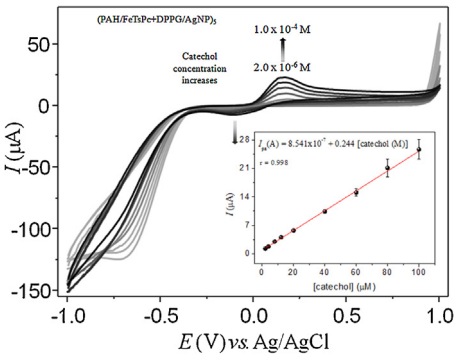

Fig. 9. cyclic voltammogram of $(PAH/FeTsPc + DPPG/AgNP)_5$ LbL film immersed in catechol standard solution (2.0 μM to 100.0 μM) containing 0.1 M KCl as supporting electrolyte at 50 mV/s. *Inset*: Plot of the anodic peak current (I_{pa}) *vs* the catechol concentrations (μM).

the anodic peak (~0.83 V) ascribed to oxidation of quinine group [44,50]. The differences on the electrocatalytic effect of modified electrodes in the presence of polyphenols indicate a possible distinction between a fixed concentration of monophenol (vanillic acid), diphenol (catechol), and triphenol (gallic acid), which was evaluated by impedance spectroscopy and principal component analysis (PCA).

3.5. pH effect in catechol oxidation

The effect of pH on the electrochemical behavior of $(PAH/FeTsPc + DPPG/AgNP)_5$ LbL film immersed in 100 μM catechol was investigated by using cyclic voltammetry in a pH range of 3.0–8.5. Fig. 8 illustrates the dependence of oxidation peak current (I_{pa}) and oxidation peak potential (E_{pa}) of catechol on pH of the supporting electrolyte. The oxidation peak potential shifted to lower potential by increasing pH (3–7), which occurs due to deprotonation step involved in the diphenol oxidation process [51]. The deprotonation is facilitated at higher pH, and can favor the electrochemical reduction of diphenol groups. However, the $(PAH/FeTsPc + DPPG/AgNP)_5$ LbL film showed a better electroactivity for the catechol oxidation in solution with pH between 5 and 7, which had the maximum anodic peak currents. The pH up 7.0 increases the amount of hydroxyl ion in solution, which may decrease the adsorption capacity of the catechol on the LbL film surface. In addition, up pH 2.9 the DPPG molecules are ionized (pKa 2.9) [52,53], which can increase the negative characteristic of the film. This latter can also decrease the adsorption capacity of the catechol on LbL film surface in pH high than 7.0 (DPPG highly ionized).

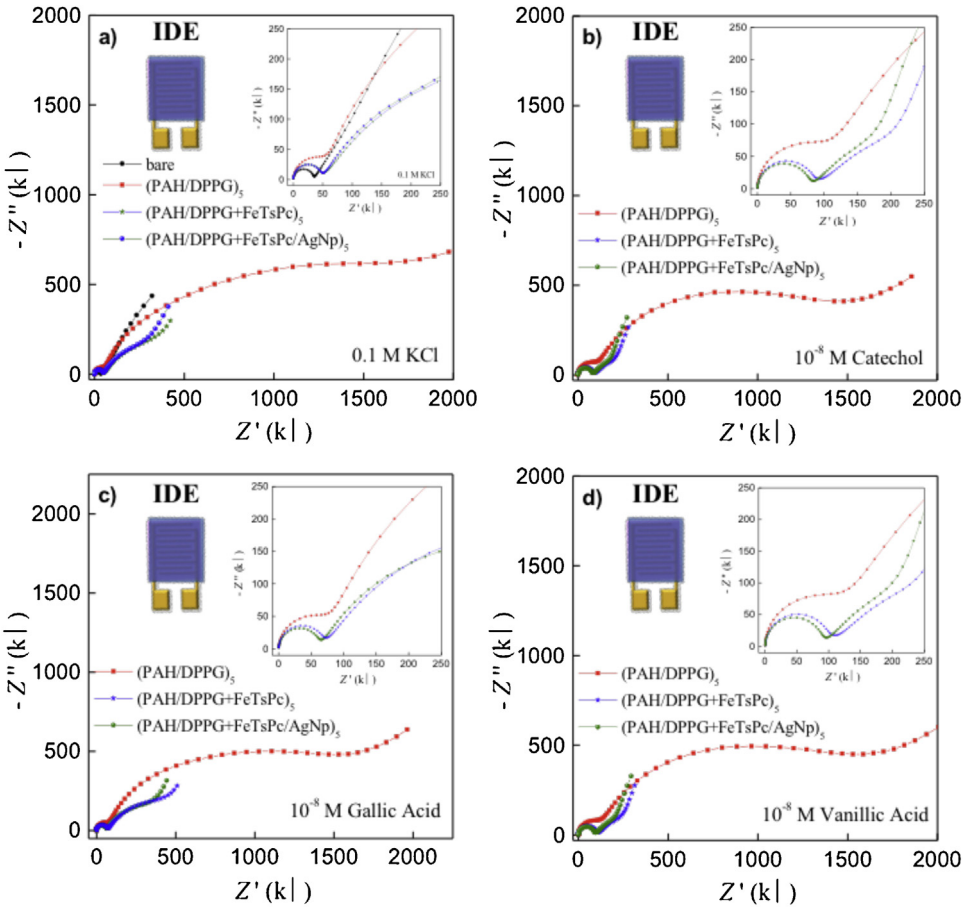

Fig. 10. (a) Nyquist plot to the impedance response for all sensing units (IDE modified with $(PAH/DPPG)_5$, $(PAH/FeTsPc + DPPG)_5$ and $(PAH/FeTsPc + DPPG/AgNp)_5$ LbL films) immersed in (a) ultrapure water and in 10^{-8} M of (b) catechol, (c) gallic acid and (d) vanillic acid standard solution (polyphenol solutions were prepared with ultrapure water). *Insets*: Schematic representation of IDE and magnifications of the high frequency range.

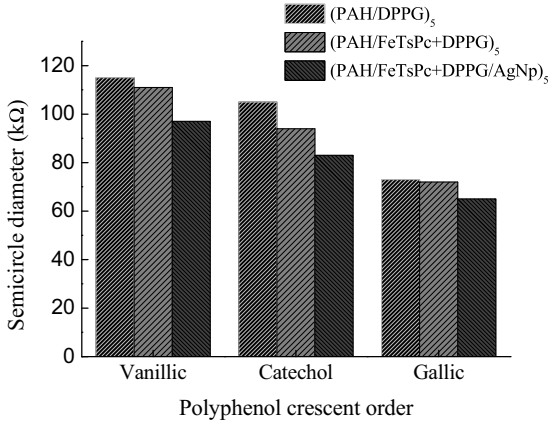

Fig. 11. Semicircle diameter in high frequency range from the impedance spectra obtained to $(PAH/DPPG)_5$, $(PAH/FeTsPc + DPPG)_5$, and $(PAH/FeTsPc + DPPG/AgNp)_5$ LbL films in Vanillic acid, catechol, and Gallic acid solution (mono- < di- < triphenol).

3.6. Sensing application

3.6.1. Cyclic voltammetry: concentration range, LOD, LOQ, repeatability, reproducibility and stability in catechol standard solution

The sensing evaluation of the ITO electrode modified with $(PAH/FeTsPc + DPPG/AgNP)_5$ LbL films was carried out in catechol standard solution with concentration of 2.0, 4.0, 6.0, 8.0, 12, 20, 40, 60, 80 and 100.0 μM (Fig. 9). The anodic peak from catechol oxidation was proportional the catechol concentrations of 2.0 μM to 100.0 μM with the regression equation of $I_{pa}(A) = 8.541 \times 10^{-7} + 0.244$ [catechol (M)], with a limit of detection (LOD) of 0.87 μM and a limit of quantification (LOQ) of 2.9 μM. The LOD and LOQ were calculated according to (3*x* blank SD)/slope and (10*x* blank SD)/slope criterion, respectively. The LOD obtained was similar of voltammetric biosensors [44], as well as the distinction between the types of polyphenols (results from cyclic voltammetry and impedance measurements) indicates a possible application of the $(PAH/FeTsPc + DPPG/AgNP)_5$ LbL film as a biomimetic sensor for diphenol compounds like catechol. The analytical performance obtained in the present work was also compared with other modified electrodes, being the oxidation peak potential, linear range, and LOD in catechol solution are listed in Table 3. The results are satisfactory to the application of $(PAH/FeTsPc + DPPG/AgNP)_5$ LbL film as catechol sensor.

The repeatability of $(PAH/FeTsPc + DPPG/AgNP)_5$ LbL film was studied in 100 μM catechol solution, obtaining a standard deviation of 3.9% for 17 successive assays. Three $(PAH/FeTsPc + DPPG/AgNP)_5$ LbL films (prepared independently) were also evaluated in the same conditions of the catechol solution, and an acceptable reproducibility with a standard deviation of 9.3% was obtained. After 20 days stored, the $(PAH/FeTsPc + DPPG/AgNP)_5$ LbL film shows only a small decrease in oxidation peak current was observed with the signal change of 10.5%.

Table 3
Comparison of analytical performances at $(PAH/FeTsPc + DPPG/AgNp)_5$ for the detection of catechol.

Film	Detection technique	E_{pa}/V (catechol)	Linear range (μM)	LOD (μM)	Ref.
$(FePc + DMPA)_{10}$[a]	Cyclic voltammetry	0.22	3–144	0.43	[62]
$(LuPc_2 + DMPA)_{10}$[b]	Cyclic voltammetry	0.14	3–144	0.33	[62]
$(CMWNTs\text{-}NHCH_2CH_2NH)_6/GCE$[c]	DPV		10–120	1.0	[63]
PEDOT/CPE[d]	DPV	0.25	1–250	0.50	[64]
PEDOT/CPE	Amperometry	0.25	0.52–4900	1.60	[64]
MnPc-His/CPE[e]	Amperometry	0	20–130	1.10	[65]
PDA-Lac-NiCNFs/MGCE[f]	Amperometry	0.40	1–9100	0.69	[66]
$(PAH/FeTsPc + DPPG/AgNp)_5$	Cyclic voltammetry	0.16	2–100	0.87	This work

[a] FePc = iron phthalocyanine, DMPA = phospholipid dimyristoyl phosphatidic acid.
[b] $LuPc_2$ = bisphthalocyanine.
[c] CMWNTs = carboxylated multi-wall carbon nanotubes, $NHCH_2CH_2NH$ = carbodiimide, GCE = glassy carbon electrode.
[d] PEDOT = poly(3,4-ethylenedioxythiophene), CPE = carbon paste electrode.
[e] MnPc = manganese phthalocyanine, His = histidine.
[f] PDA = polydopamine, Lac = lacase enzyme, NiCNFs = nickel nanoparticles loaded carbon nanofibers, MGCE = magnetic glassy carbon electrode.

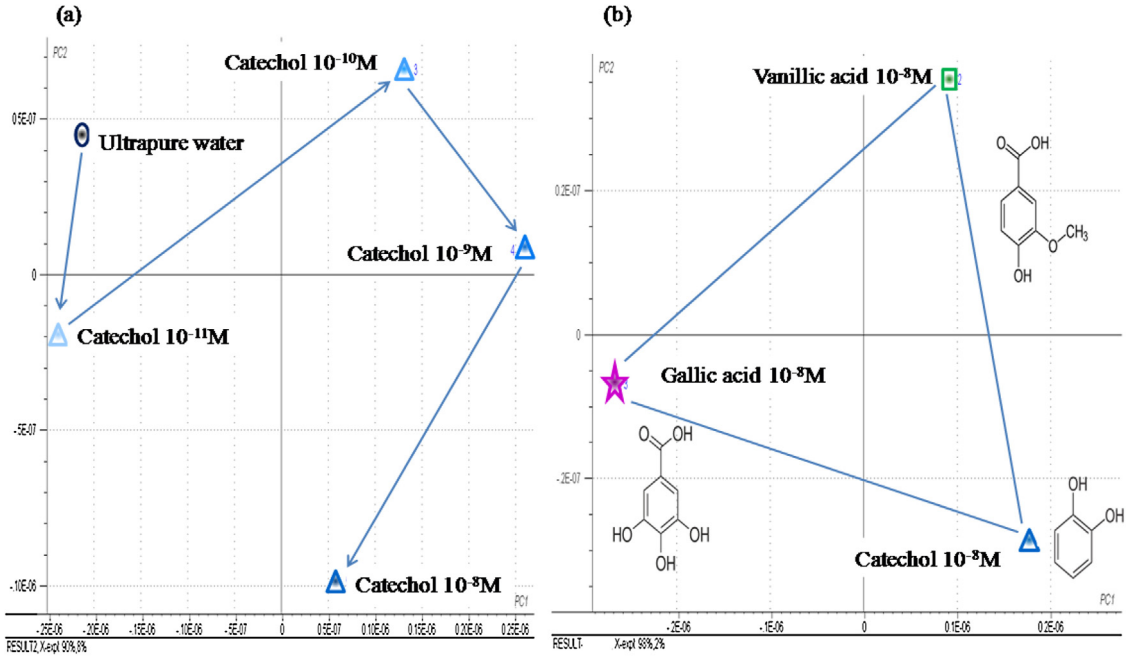

Fig. 12. PCA plot for capacitance curves for all sensing units (IDE unmodified, IDE modified with $(PAH/DPPG)_5$, $(PAH/FeTsPc + DPPG)_5$ and $(PAH/FeTsPc + DPPG/AgNp)_5$ LbL films) immersed into ultrapure water and aqueous solutions of (a) catechol (10^{-11}, 10^{-10}, 10^{-9} and 10^{-8} M) and (b) 10^{-8} M catechol, 10^{-8} M vanillic acid and 10^{-8} M gallic acid.

3.6.2. Impedance spectroscopy

The sensorial analysis by impedance spectroscopy was carried out using platinum interdigitated electrodes containing: $(PAH/DPPG)_5$, $(PAH/FeTsPc + DPPG)_5$ and $(PAH/FeTsPc + DPPG/AgNP)_5$ LbL films. The sensing array composed of these 3 sensing units was used to detect low catechol concentrations (10^{-11}–10^{-8} M). Furthermore, the distinction between a fixed concentration of catechol (diphenol), vanillic acid (monophenol) and gallic acid (triphenol) was also tested.

Fig. 10(a) shows the impedance results for all sensing units in terms of Nyquist plot immersed in ultrapure water. The result for the Pt interdigitated bare electrode was given for comparison. It can be seen that the sensing units composed of the LbL films present a similar behavior in terms of the impedance response, but different from the bare electrode. The main difference observed in the electrical response of the sensing units is in the region at low frequency, i.e. in the double layer region according to Taylor and MacDonald model [54]. Briefly, the theoretical model based on the electrical equivalent circuit proposed by Taylor and MacDonald claims that changes in capacitance for each frequency range is attributed to different phenomena, namely: double layer effects at low frequencies (<50 Hz), film effects in intermediate frequencies (10^2–10^4 Hz) and electrode geometry effects at high frequencies (>10^5 Hz). [54]. In this work, the main factors that could influence the double layer structuration (since the same electrolyte is used) are (i) different surface areas promoted by the films, and/or (ii) different distances between ion-surface due to the electrostatic characteristic of the films. The impedance values at low frequency increases in the order: $(PAH/FeTsPc + DPPG/AgNP)_5 < (PAH/FeTsPc + DPPG)_5$. It makes sense, once the AgNPs have conductive and DPPG insulating properties.

In Fig. 10(b)–(d) we can observe the Nyquist plot of all sensing units for the analyzed solutions, which changes indicate that sensing units are capable of detecting the tested analytes. All impedance spectra show a semicircle in the high frequency, region characteristic of kinetic control of the charge-transfer process. However, for $(PAH/FeTsPc + DPPG/AgNP)_5$ films in catechol solution a smaller semicircle diameter (charge transfer resistance) was observed. The latter can be ascribed to the decrease of resistance of charge transfer promoted by the nanoparticles, i.e., the charge transfer is favored by the incorporation of AgNp on the LbL films. Moreover, the LbL films with FeTsPc show a similar behavior and higher sensibility to polyphenol concentration than LbL films composed of phospholipids only. The latter can be ascribed to axial coordination

between the metal center from phthalocyanines and OH groups of polyphenols. This confirms that structural similarity between metallic phthalocyanines and the heme prosthetic group of the enzymes promotes the biomimetic properties of metallic phthalocyanines.

A dependence of semicircle diameter at low frequency with the amount of OH groups from vanillic acid, catechol, and gallic acid was observed. The semicircle diameter for each sensorial unit decreases in crescent order OH group amount (mono- < di- < triphenol), as shown in Fig. 11, which indicates that kinetic process is favored by the increasing OH groups. This behavior was observed for all sensorial units. The results demonstrate that the charge transfer (kinetic control) in IDE interface is directly proportional to the amount of groups involved in this process (in this case the OH groups) and not to the size or molecular weight of the polyphenols (in increasing order: catechol (110, 1 g/mol) <vanillic acid (168, 2 g/mol) <gallic acid (170, 2 g/mol)).

A practical way to visualize the sensing array responses to the different solutions is to combine the individual responses for each sensing unit with a statistical method. In the case of the array of sensors used here, forming an "electronic tongue", it has been common to use the method of PCA (principal component analysis) [55,56]. In the case of our work, the entire capacitance curves were used to generate such a correlation in order to avoid losing information that could be relevant for discrimination. So, each cluster in a PCA diagram corresponds to the response of all sensing units, providing a more comprehensive analysis of the electronic tongue. Fig. 12(a) and (b) shows clearly the distinction between the cluster for different concentrations of catechol and further the distinction among catechol, gallic acid, and vanillic acid solutions. In Fig. 12(a) for different catechol concentrations, the First Principal Component (PC1) explains the 90% of the information and Second Principal Component (PC2) the 8%. Fig. 12(b)for different polyphenols the PC1 explains the 97% of the information and PC2 the 2%. It is important to notice that with only two principal components, the percentage of explained variance was 98 and 99%. It can be concluded that the sensors are able to distinguish between the catechol concentrations and different antioxidants. This sensor array shows a high sensitivity, capable of detecting concentrations of 10^{-10} M of catechol, which is comparable to enzymatic biosensors [57].

3.6.3. *Analysis in green tea sample by cyclic voltammetry*

The amount of polyphenol in a green tea sample was performed by standard addition using catechol as standard. The cyclic voltammetry of LbL $(PAH/FeTsPc + DPPG/AgNP)_5$ films in green tea sample showed three anodic peaks between 0.1 and 0.5 V, which are ascribed to different flavan-3-ols high present in herbs from *Camellia Sinensis* [58]. The addition of catechol standard showed an increase of potential peak at 0.2 V. Thus, the polyphenol concentration obtained of 270 mg/L corresponding to all polyphenol species that are oxidized in the same potential (polyphenol containing catechol group). Through the Folin-Ciocalteu method, the polyphenol concentration corresponds to 900 mg/L. The difference between the methods can be ascribed to reactivity non-selective of the phosphotungstate-molybdate reagent of Folin-Ciocalteau, which reacts with all natural phenol species present in the tea samples. The polyphenol concentration of 270 mg/L corresponds to 30% of total polyphenol from Folin-Ciocalteu, which is agreement with the amount of anodic peak observed by cyclic voltammogram.

4. Conclusions

The thin films with bilayers of $(PAH/FeTsPc + DPPG)_n$ or trilayers of $(PAH/FeTsPc + DPPG/AgNP)_n$ were successfully obtained by LbL technique. The morphology shows that LbL films are homogeneous at micro and nanoscales, with small aggregates observed only to PAH/FeTsPc + DPPG/AgNP LbL film, ascribed to the presence of AgNP. The AgNPs immobilization allowed obtaining SERS and SERRS spectra, which can be further applied as a complementary sensing tool. FTIR measurements confirm that the growth of LbL films containing bi- and trilayers are governed by the electrostatic interaction between PAH, FeTsPc, and DPPG molecules. The PAH/FeTsPc + DPPG/AgNP LbL film showed an enhancing electrocatalytic activity toward oxidation of catechol. The AgNP favored the direct electron transfer between for FeTsPc and electrode surface. The voltammetric measurements using the $(PAH/FeTsPc + DPPG/AgNP)_5$ LbL film presented a linear range for catechol concentration from 0.2 to 100 μM, with a limit of detection of 0.87 μM. The LbL films also showed good sensibility as an electronic tongue to detect catechol in aqueous solution, with concentration range similar to biosensors. Furthermore, the impedance measurements associated with principal component analysis was an efficient approach to distinguish different catechol concentrations as well as catechol, gallic and vanillic acid solutions. The sensor proposed can be widely applied to quantitative analysis of polyphenol in natural tea extracts without pretreatment of the samples. The experimental results from cyclic voltammetry show a polyphenol quantification of 30% in relation to results obtained with Folin-Ciocalteu method. Thus, this sensor includes the determination of catechol derivatives in vegetable samples.

Acknowledgments

Financial support by MINECO and FEDER (grant CICYT-AGL2015-67482-R) and the Junta de Castilla y León (VA-032U13) is gratefully acknowledged from Spain and FAPESP, CNPq and CAPES from Brazil.

References

[1] V.R. Preedy, Tea in Health and Disease Prevention, Academic Press, 2013.
[2] A.J. Queimada, F.L. Mota, S.P. Pinho, E.A. Macedo, Solubilities of biologically active phenolic compounds: measurements and modeling (vol. 113, pg. 3473, 2009), J. Phys. Chem. B 113 (2009) 6582.
[3] C.M. Santana, Z.S. Ferrera, M.E. Padron, J.J. Rodriguez, Methodologies for the extraction of phenolic compounds from environmental samples: new approaches, Molecules 14 (2009) 298–320.
[4] M.N. Karim, J.E. Lee, H.J. Lee, Amperometric detection of catechol using tyrosinase modified electrodes enhanced by the layer-by-layer assembly of gold nanocubes and polyelectrolytes, Biosens. Bioelectron. 61 (2014) 147–151.
[5] N. Kobayashi, P. Janda, A.B.P. Lever, Cathodic reduction of oxygen and hydrogen-peroxide at cobalt and iron crowned phthalocyanines adsorbed on highly oriented pyrolytic-graphite electrodes, Inorg. Chem. 31 (1992) 5172–5177.
[6] M.D.T. Sotomayor, A.A. Tanaka, L.T. Kubota, Development of an enzymeless biosensor for the determination of phenolic compounds, Anal. Chim. Acta 455 (2002) 215–223.
[7] E.G.R. Fernandes, L.C. Brazaca, M.L. Rodriguez-Mendez, J.A. de Saja, V. Zucolotto, Immobilization of lutetium bisphthalocyanine in nanostructured biomimetic sensors using the LbL technique for phenol detection, Biosens. Bioelectron. 26 (2011) 4715–4719.
[8] W.J.R. Santos, P.R. Lima, C.R.T. Tarley, L.T. Kubota, Synthesis, characterization and kinetics of catalytically active molecularly imprinted polymers for the selective recognition of 4-aminophenol, J. Brazil. Chem. Soc. 20 (2009) 820–825.
[9] S. Casillia, M. De Luca, C. Apetrei, V. Parra, A.A. Arrieta, L. Valli, et al., Langmuir-Blodgett and Langmuir-Schaefer films of homoleptic and heteroleptic phthalocyanine complexes as voltammetric sensors: applications to the study of antioxidants, Appl. Surf. Sci. 246 (2005) 304–312.
[10] A.B.P. Lever, The phthalocyanines – molecules of enduring value; a two-dimensional analysis of redox potentials, J. Porphyr. Phthalocyanines 3 (1999) 488–499.
[11] T. Nyokong, E. Antunes, Influence of nanoparticle materials on the photophysical behavior of phthalocyanines, Coord. Chem. Rev. 257 (2013) 2401–2418.
[12] V.P. Chauke, W. Chidawanyika, T. Nyokong, The electrochemical behavior of gold nanoparticle-Tantalum(V) phthalocyanine composites: applications towards the electroanalysis of Bisphenol A, Electroanalysis 23 (2011) 487–496.

[13] C. Medina-Plaza, L.N. Furini, C.J.L. Constantino, J.A. de Saja, M.L. Rodriguez-Mendez, Synergistic electrocatalytic effect of nanostructured mixed films formed by functionalised gold nanoparticles and bisphthalocyanines, Anal. Chim. Acta 851 (2014) 95–102.
[14] P.H.B. Aoki, P. Alessio, L.N. Furini, C.J.L. Constantino, T.T.A.T. Neves, F.V. Paulovich, et al., Molecularly designed layer-by-layer (LbL) films to detect catechol using information visualization methods, Langmuir 29 (2013) 7542–7550.
[15] P. Alessio, P.H.B. Aoki, J.A.D. Saez, M.L. Rodriguez-Mendez, C.J.L. Constantino, Combining SERRS and electrochemistry to characterize sensors based on biomembrane mimetic models formed by phospholipids, RSC Adv. 1 (2011) 211–218.
[16] P.H.B. Aoki, P. Alessio, J.A. De Saja, C.J.L. Constantino, Incorporation of Ag nanoparticles into membrane mimetic systems composed by phospholipid layer-by-layer (LbL) films to achieve surface-enhanced Raman scattering as a tool in drug interaction studies, J. Raman Spectrosc. 41 (2010) 40–48.
[17] P.H.B. Aoki, D. Volpati, A. Riul, W. Caetano, C.J.L. Constantino, Layer-by-layer technique as a new approach to produce nanostructured films containing phospholipids as transducers in sensing applications, Langmuir 25 (2009) 2331–2338.
[18] P.C. Lee, D. Meisel, Adsorption and surface-enhanced raman of dyes on silver and gold sols, J. Phys. Chem.—US 86 (1982) 3391–3395.
[19] P. Alessio, M.L. Rodriguez-Mendez, J.A.D. Saez, C.J.L. Constantino, Iron phthalocyanine in non-aqueous medium forming layer-by-layer films: growth mechanism, molecular architecture and applications, Phys. Chem. Chem. Phys. 12 (2010) 3972–3983.
[20] K. Kneipp, D. Fassler, Sers excitation profile investigation of a cyanine dye adsorbed on silver colloidal particles, Chem. Phys. Lett. 106 (1984) 498–502.
[21] P. Hildebrandt, M. Stockburger, Surface-enhanced resonance Raman-spectroscopy of rhodamine-6 g adsorbed on colloidal silver, J. Phys. Chem.—US 88 (1984) 5935–5944.
[22] Y. Wang, S.K. Eswaramoorthy, L.J. Sherry, J.A. Dieringer, J.P. Camden, G.C. Schatz, et al., A method to correlate optical properties and structures of metallic nanoparticles, Ultramicroscopy 109 (2009) 1110–1113.
[23] R.A. Alvarez-Puebla, E. Arceo, P.J.G. Goulet, J.J. Garrido, R.F. Aroca, Role of nanoparticle surface charge in surface-enhanced Raman scattering, J. Phys. Chem. B 109 (2005) 3787–3792.
[24] W.S. Alencar, F.N. Crespilho, M.R.M.C. Santos, V. Zucolotto, O.N. Oliveira, W.C. Silva, Influence of film architecture on the charge-transfer reactions of metallophthalocyanine layer-by-layer films, J. Phys. Chem. C 111 (2007) 12817–12821.
[25] R.A.D. Luz, M.V.A. Martins, J.L. Magalhaes, J.R. Siqueira, V. Zucolotto, O.N. Oliveira, et al., Supramolecular architectures in layer-by-layer films of single-walled carbon nanotubes, chitosan and cobalt(II) phthalocyanine, Mater. Chem. Phys. 130 (2011) 1072–1077.
[26] M. Gamella, S. Campuzano, A.J. Reviejo, J.M. Pingarron, Electrochemical estimation of the polyphenol index in wines using a laccase biosensor, J. Agr. Food Chem. 54 (2006) 7960–7967.
[27] D. Volpati, P. Alessio, A.A. Zanfolim, F.C. Storti, A.E. Job, M. Ferreira, et al., Exploiting distinct molecular architectures of ultrathin films made with iron phthalocyanine for sensing, J. Phys. Chem. B 112 (2008) 15275–15282.
[28] W.A. Nevin, W. Liu, M. Melnik, A.B.P. Lever, Spectroelectrochemistry of cobalt and iron tetrasulfonated phthalocyanines, J. Electroanal. Chem. 213 (1986) 217–234.
[29] C. Ercolani, M. Gardini, F. Monacelli, G. Pennesi, G. Rossi, Interaction of (Phthalocyaninato)Iron(Ii) with molecular-Oxygen – synthesis and characterization of 2 different crystalline forms of (Mu-Oxo)Bis((Phthalocyaninato)Iron(Iii)), Inorg. Chem. 22 (1983) 2584–2589.
[30] R. Dieing, G. Schmid, E. Witke, C. Feucht, M. Dressen, J. Pohmer, et al., Soluble substituted Mu-Oxo(Phthalocyaninato)Iron(Iii) Dimers, Chem. Ber. 128 (1995) 589–598.
[31] C.A.S. Barbosa, P.M. Dias, A.M.D. Ferreira, V.R.L. Constantino, Mg-Al hydrotalcite-like compounds containing iron-phthalocyanine complex: effect of aluminum substitution on the complex adsorption features and catalytic activity, Appl. Clay Sci. 28 (2005) 147–158.
[32] P. Alessio, C.J.L. Constantino, R.F. Aroca, O.N. Oliveira, Surface-Enhanced Raman scattering: metal nanostructures coated with Langmuir-Blodgett films, J. Chil. Chem. Soc. 55 (2010) 469–478.
[33] L.N. Furini, E. Feitosa, P. Alessio, M.H. Shimabukuro, A. Riul, C.J.L. Constantino, Tuning the nanostructure of DODAB/nickel tetrasulfonated phthalocyanine bilayers in LbL films, Mater. Sci. Eng. C-Mater. 33 (2013) 2937–2946.
[34] Z.Q. Liu, X.X. Zhang, Y.X. Zhang, J.Z. Jiang, Theoretical investigation of the molecular, electronic structures and vibrational spectra of a series of first transition metal phthalocyanines, Spectrochim. Acta A 67 (2007) 1232–1246.
[35] V. Zucolotto, M. Ferreira, M.R. Cordeiro, C.J.L. Constantino, D.T. Balogh, A.R. Zanatta, et al., Unusual interactions binding iron tetrasulfonated phthalocyanine and poly(allylamine hydrochloride) in layer-by-layer films, J. Phys. Chem. B 107 (2003) 3733–3737.
[36] J.J. Laserna, Modern Techniques in Raman Spectroscopy, Wiley, 1996.
[37] P. Corio, J.C. Rubim, R. Aroca, Contribution of the Herzberg-Teller mechanism to the surface-enhanced Raman scattering of iron phthalocyanine adsorbed on a silver electrode, Langmuir 14 (1998) 4162–4168.
[38] L. Gaffo, C.J.L. Constantino, W.C. Moreira, R.F. Aroca, O.N. Oliveira, Surface-enhanced Raman scattering and micro-Raman imaging of Langmuir-Blodgett films of rhodium phthalocyanine, Spectrochim. Acta A 60 (2004) 321–327.
[39] P.H.B. Aoki, D. Volpati, F.C. Cabrera, V.L. Trombini, A. Riul, C.J.L. Constantino, Spray layer-by-layer films based on phospholipid vesicles aiming sensing application via e-tongue system, Mater. Sci. Eng. C-Mater. 32 (2012) 862–871.
[40] S. Zecevic, B. Simicglavaski, E. Yeager, A.B.P. Lever, P.C. Minor, Spectroscopic and electrochemical studies of transition-metal tetrasulfonated phthalocyanines. 5. voltammetric studies of adsorbed tetrasulfonated phthalocyanines (Mtspc) in aqueous-solutions, J. Electroanal. Chem. 196 (1985) 339–358.
[41] J.A.P. Chaves, M.F.A. Araujo, J.D.G. Varela, A.A. Tanaka, Eletrocatalysis of the oxygen reduction reaction on graphite electrodes modified with iron tetracarboxyphthalocyanine, Ecletica. Quim. 28 (2003) 9–19.
[42] F. Bedioui, S. Griveau, T. Nyokong, A.J. Appleby, C.A. Caro, M. Gulppi, et al., Tuning the redox properties of metalloporphyrin- and metallophthalocyanine-based molecular electrodes for the highest electrocatalytic activity in the oxidation of thiols, Phys. Chem. Chem. Phys. 9 (2007) 3383–3396.
[43] F.N. Crespilho, R.M. Iost, S.A. Travain, O.N. Oliveira, V. Zucolotto, Enzyme immobilization on Ag nanoparticles/polyaniline nanocomposites, Biosens. Bioelectron. 24 (2009) 3073–3077.
[44] C. Apetrei, P. Alessio, C.J.L. Constantino, J.A. de Saja, M.L. Rodriguez-Mendez, F.J. Pavinatto, et al., Biomimetic biosensor based on lipidic layers containing tyrosinase and lutetium bisphthalocyanine for the detection of antioxidants, Biosens. Bioelectron. 26 (2011) 2513–2519.
[45] T.W. Hui, K.Y. Wong, K.K. Shiu, Kinetics of *o*-benzoquinone mediated oxidation of glucose by glucose oxidase at edge plane pyrolytic graphite electrode, Electroanalysis 8 (1996) 597–601.
[46] L.F. Chen, H.Q. Xie, J. Li, Electrochemical glucose biosensor based on silver nanoparticles/multiwalled carbon nanotubes modified electrode, J. Solid State Electrochem. 16 (2012) 3323–3329.
[47] A. Szydlowska-Czerniak, A. Tulodziecka, E. Szlyk, A silver nanoparticle-based method for determination of antioxidant capacity of rapeseed and its products, Analyst 137 (2012) 3750–3759.
[48] J. Tashkhourian, S.F. Nami-Ana, A sensitive electrochemical sensor for determination of gallic acid based on SiO2 nanoparticle modified carbon paste electrode, Mater. Sci. Eng. C-Mater. 52 (2015) 103–110.
[49] R. Abdel-Hamid, E.F. Newair, Electrochemical behavior of antioxidants: I. Mechanistic study on electrochemical oxidation of gallic acid in aqueous solutions at glassy-carbon electrode, J. Electroanal. Chem. 657 (2011) 107–112.
[50] C. Apetrei, I.M. Apetrei, J.A. De Saja, M.L. Rodriguez-Mendez, Carbon paste electrodes made from different carbonaceous materials: application in the study of antioxidants, Sensors-Basel 11 (2011) 1328–1344.
[51] H.L. Qi, C.X. Zhang, Simultaneous determination of hydroquinone and catechol at a glassy carbon electrode modified with multiwall carbon nanotubes, Electroanalysis 17 (2005) 832–838.
[52] J. Minones, P. Dynarowicz-Latka, J. Minones, J.M.R. Patino, E. Iribarnegaray, Orientational changes in dipalmitoyl phosphatidyl glycerol Langmuir monolayers, J. Colloid Interface Sci. 265 (2003) 380–385.
[53] G. Cevc, D. Marsh, Phospholipid Bilayers: Physical Principles and Models, Wiley, 1987.
[54] D.M. Taylor, A.G. Macdonald, Ac admittance of the metal-Insulator-electrolyte interface, J. Phys. D Appl. Phys. 20 (1987) 1277–1283.
[55] A. Riul, D.S. dos Santos, K. Wohnrath, R. Di Tommazo, A.C.P.L.F. Carvalho, F.J. Fonseca, et al., Artificial taste sensor: efficient combination of sensors made from Langmuir-Blodgett films of conducting polymers and a ruthenium complex and self-assembled films of an azobenzene-containing polymer, Langmuir 18 (2002) 239–245.
[56] M. Khaydukova, X. Ceto, D. Kirsanov, M. del Valle, A. Legin, A tool for general quality assessment of black tea-retail price prediction by an electronic tongue, Food Anal. Method 8 (2015) 1088–1092.
[57] V. Zucolotto, A.P.A. Pinto, T. Tumolo, M.L. Moraes, M.S. Baptista, A. Riul, et al., Catechol biosensing using a nanostructured layer-by-layer film containing Cl-catechol 1 2-dioxygenase, Biosens. Bioelectron. 21 (2006) 1320–1326.
[58] D.A. Balentine, S.A. Wiseman, L.C.M. Bouwens, The chemistry of tea flavonoids, Crit. Rev. Food Sci. 37 (1997) 693–704.
[59] A. Dicko, H. Bourque, M. Pezolet, Study by infrared spectroscopy of the conformation of dipalmitoylphosphatidylglycerol monolayers at the air-water interface and transferred on solid substrates, Chem. Phys. Lipids 96 (1998) 125–139.
[60] G. Mao, J. Desai, C.R. Flach, R. Mendelsohn, Structural characterization of the monolayer-multilayer transition in a pulmonary surfactant model: IR studies of films transferred at continuously varying surface pressures, Langmuir 24 (2008) 2025–2034.
[61] K.O. Kwon, M.J. Kim, M. Abe, T. Ishinomori, K. Ogino, Thermotropic behavior of a phospholipid-bilayer interacting with metal-Ions, Langmuir 10 (1994) 1415–1420.
[62] P. Alessio, F.J. Pavinatto, O.N. Oliveira, J.A.D. Saez, C.J.L. Constantino, M.L. Rodriguez-Mendez, Detection of catechol using mixed Langmuir-Blodgett films of a phospholipid and phthalocyanines as voltammetric sensors, Analyst 135 (2010) 2591–2599.
[63] S.Q. Feng, Y.Y. Zhang, Y.M. Zhong, Y.C. Li, S.X. Li, Simultaneous determination of hydroquinone and catechol using covalent layer-by-layer self-assembly of carboxylated-MWNTs, J. Electroanal. Chem. 733 (2014) 1–5.
[64] Y.H. Song, T. Yang, X.F. Zhou, H.T. Zheng, S. Suye, A microsensor for hydroquinone and catechol based on a poly(3,4-ethylenedioxythiophene) modified carbon fiber electrode, Anal. Methods—UK 8 (2016) 886–892.

[65] W.D.R. Santos, A.L. Sousa, M.D.T. Sotomayor, F.S. Damos, S.M.C.N. Tanaka, L.T. Kubota, et al., Manganese phthalocyanine as a biomimetic electrocatalyst for phenols in the development of an amperometric sensor, J. Brazil. Chem. Soc. 20 (2009) 1180–1187.
[66] D.W. Li, L. Luo, Z.Y. Pang, L. Ding, Q.Q. Wang, H.Z. Ke, et al., Novel phenolic biosensor based on a magnetic polydopamine-laccase-nickel nanoparticle loaded carbon nanofiber composite, ACS Appl. Mater. Interfaces 6 (2014) 5144–5151.

Biographies

Priscila Alessio has a degree in Physics from Univ Estadual Paulista (UNESP – Brazil), MSc and Ph.D. in Science and Technology of Materials (POSMAT) from the same university and Ph.D. in Physical Sciences from University of Valladolid (Spain). She is now a post-doctoral researcher at UNESP focusing on sensors, mainly those based on electrical impedance spectroscopy with nanostructured films as transducer elements (electronic-tongue type). She is author or co-author of 28 publications and two book chapters.

Cibely Silva Martin has a degree and MSc in chemistry from Univ Estadual Paulista (UNESP – Brazil). At present, she is a postgraduate student (doctoral) in Science and Technology of Materials (POSMAT) at the Department of Physics of the University of State of Sao Paulo (UNESP). Her research is focusing on electrochemical sensors, mainly those based on nanostructured films. She is author or co-author of 15 publications.

José Antonio de Saja Sáez was born in Miranda de Ebro (Spain), in 1940. He is a professor and head of the Department of Condensed Matter Physics at the University of Valladolid. His present research interest is at the intersection of materials science, physics, physical chemistry and device engineering and focuses on novel nanostructured materials (mainly from LB monolayers). At the present moment, he coordinating a Project devoted to the development of an electronic nose, an electronic tongue and an electronic eye for the assessment of the organoleptic characteristics of wines and olive oils. He is author or co-author of over 320 publications and has edited ten books.

María Luz Rodríguez-Méndez received the Ph.D. in chemistry from the University of Valladolid (Spain) in 1990. In 1996, she obtained a permanent Professor position at the University of Valladolid and in 2011 she has obtained the habilitation and the Chair of Inorganic Chemistry at the Industrial Engineers School of the University of Valladolid. Her main current interest is in the development of gas and liquid nanostructured sensors based on phthalocyanines and on conducting polymers. She is also an expert in the development of electrochemical nanobiosensors. She is author or co-author of over 110 publications, four books, and three patents.